

*Supporting Information*

**Cobalt Pincer Complexes in Catalytic C-H Borylation: The  
Pincer Ligand Flips Rather Than Dearomatizes**

Haixia Li<sup>1</sup>, Jennifer V. Obligacion<sup>2</sup>, Paul J. Chirik<sup>2</sup>, and Michael B. Hall<sup>1\*</sup>

<sup>1</sup>*Department of Chemistry, Texas A&M University, College Station, Texas 77843, United States*

<sup>2</sup>*Department of Chemistry, Princeton University, Princeton, New Jersey 08544, United States*

**Corresponding Author**

\* [mbhall@tamu.edu](mailto:mbhall@tamu.edu)

## Table of Contents

SI1. Verification of ground states of four-coordinate cobalt species .....	3
SI2. Optimized geometries of some species involved in Figure 2 .....	7
SI3. The superimposed structures of the optimized geometry of 2 and its X-ray crystal structure .....	7
SI4. An alternative pathway for the formation of 4 from 2 .....	8
SI5. Formation of the isomer of 9 .....	8
SI6. Isomerization of 4 to its isomer .....	9
SI7. Results for the release of H <sub>2</sub> from the <i>trans</i> -dihydride Co-complex with model systems .....	10
SI8. Verification of $\omega$ B97XD/Def2TZVP(SMD)// $\omega$ B97XD/BS4 .....	16
SI9. Optimized geometries of transition states for the release of H <sub>2</sub> from 2 <sup>Ir</sup> , 2 <sup>Ph</sup> , 2 <sup>Ir-Ph</sup> , and 2 <sup>Ir-Ph-tBu</sup> .....	17
SI10. A possible pathway for the formation of the active species from the catalyst precursor with model systems .....	18
SI11. Alternative pathways for the addition of C <sub>6</sub> H <sub>6</sub> to the cobalt boryl species with model systems.....	19
SI12. Comparisons of transition state TS <sub>11-13</sub> and that for the formation of 15 and its isomer .....	21
SI13. Addition of C <sub>6</sub> H <sub>6</sub> to corresponding Rh and Ir complexes.....	22
SI14. Optimized geometries for the species in Figure 6 in the text.....	24
SI15. Results for the reductive elimination of the B-C bond with model systems .....	25
SI16. Optimized geometries of the species in Figure 7 .....	30
SI17. Results for the regeneration of the active species with model systems.....	32

## SI1. Verification of ground states of four-coordinate cobalt species

In experiments, the cobalt alkyl complex **1**, (<sup>i</sup>PrPNP)Co(CH<sub>2</sub>SiMe<sub>3</sub>), was isolated and confirmed to be diamagnetic (singlet state) with four substituents around Co in a planar geometry. In addition, other possible structures, such as a triplet and open shell singlet state with four substituents around Co in a planar geometry (**1<sup>T</sup>** and **1<sup>Os</sup>**), and a triplet state with four substituents around Co in a nearly tetrahedral geometry (**1<sup>T-Td</sup>**), were also considered. Geometries were optimized in gas phase at the level of  $\omega$ B97XD/BS2 (cc-pVDZ&LANL2DZ(Co)). The solvent effects were then considered by doing single point calculations in the experimentally used solvent toluene with the SMD solvent model at the level of  $\omega$ B97XD/BS3 (cc-pVTZ&SDD(Co)). As shown in Table S1, **1<sup>T-Td</sup>** is the most stable structure among them, which is inconsistent with the experiments. To investigate the effects of basis sets, **1** and **1<sup>T-Td</sup>** are recalculated in gas phase at the level of  $\omega$ B97XD/BS1, where atoms of the <sup>i</sup>PrPNP ligand except N and P use cc-pVDZ and the others use Def2TZVP. Then the SMD single point calculations are conducted in toluene at the level of  $\omega$ B97XD/Def2TZVP. As shown in Table S1, results at the level of  $\omega$ B97XD/Def2TZVP(SMD)// $\omega$ B97XD/BS1 are different from that at the  $\omega$ B97XD/BS3(SMD)// $\omega$ B97XD/BS2 level by several kcal/mol, and are also different from the results at the  $\omega$ B97XD/Def2TZVP(SMD)// $\omega$ B97XD/BS2 level by a few kcal/mol. Another basis set BS6, where Co uses 6-311+G\*, the methyl groups of <sup>i</sup>Pr substituents and of -CH<sub>2</sub>SiMe<sub>3</sub> ligand use 6-31G, and the others use 6-311G\*, was selected to optimize the geometries in gas phase. As shown in Table S1, the results at the level of  $\omega$ B97XD/Def2TZVP(SMD)// $\omega$ B97XD/BS6 are very close to that at the level of  $\omega$ B97XD/Def2TZVP(SMD)// $\omega$ B97XD/BS1. However,  $\omega$ B97XD underestimates the triplet state of **1<sup>T-Td</sup>**. Thus, the combinations of BS6 and Def2TZVP(SMD) are employed to test the effects of DFT functionals by computing **1**

and  $\mathbf{1}^{\text{T-Td}}$ . These DFT functionals involve hybrid functionals ( $\omega$ B97XD, M06, TPSSh) and non-hybrid functionals (TPSS, TPSS-D3 (with EmpiricalDispersion=GD3BJ), M06L, PBE). According to the results in Table S2, the TPSS functional gives reasonable results where  $\mathbf{1}^{\text{T-Td}}$  is slightly higher than  $\mathbf{1}$  by a few kcal/mol.

Table S1: Free energies in toluene ( $\Delta G_{\text{toluene}}$  in kcal/mol relative to  $\mathbf{1}$ ) for  $\mathbf{1}$ ,  $\mathbf{1}^{\text{T}}$ ,  $\mathbf{1}^{\text{OS}}$ , and  $\mathbf{1}^{\text{T-Td}}$ .

	$\mathbf{1}$	$\mathbf{1}^{\text{T}}$	$\mathbf{1}^{\text{OS}}$	$\mathbf{1}^{\text{T-Td}}$
$\omega$ B97XD/BS3(SMD)// $\omega$ B97XD/BS2	0.0	-1.6	-3.9	-21.2
$\omega$ B97XD/Def2TZVP(SMD) // $\omega$ B97XD/BS1	0.0	/	/	-14.6
$\omega$ B97XD/Def2TZVP(SMD) // $\omega$ B97XD/BS2	0.0	/	/	-12.8
$\omega$ B97XD/Def2TZVP(SMD) // $\omega$ B97XD/BS6	0.0	/	/	-14.6

Table S2: Free energies in toluene ( $\Delta G_{\text{toluene}}$  in kcal/mol) for  $\mathbf{1}$  and  $\mathbf{1}^{\text{T-Td}}$ .

	$\mathbf{1}$	$\mathbf{1}^{\text{T-Td}}$
M06/Def2TZVP(SMD)//M06/BS6	0.0	-9.6
TPSSh/Def2TZVP(SMD)//TPSSh/BS6	0.0	-8.1
TPSS/Def2TZVP(SMD)//TPSS/BS6	0.0	2.2
TPSS-D3/Def2TZVP(SMD)//TPSS-D3/BS6	0.0	5.4
M06L/Def2TZVP(SMD)//M06L/BS6	0.0	-8.3
PBE/Def2TZVP(SMD)//PBE/BS6	0.0	7.8

To further confirm the performance of TPSS and  $\omega$ B97XD, several experimentally isolated species, ( $^{\text{iPr}}$ PNP)CoCl, ( $^{\text{tBu}}$ PNP)CoCl, and ( $^{\text{tBu}}$ PNP)CoH, were investigated by using TPSS and  $\omega$ B97XD. In experiments, ( $^{\text{iPr}}$ PNP)CoCl was observed to adopt  $S = 1$  magnetic ground state with a nearly tetrahedral geometry in toluene. In contrast, ( $^{\text{tBu}}$ PNP)CoCl and ( $^{\text{tBu}}$ PNP)CoH were identified to be diamagnetic with a nearly

planar geometry, which is likely a result of steric effects of tBu substituents. TPSS and  $\omega$ B97XD were used to investigate these complexes by comparing their closed shell singlet state with a nearly planar geometry and the triplet state with a nearly tetrahedral geometry. As shown in Table S3, TPSS predicts the ground states consistent with their experiments, while  $\omega$ B97XD underestimates triplet states. Comparisons of the optimized geometries at TPSS and  $\omega$ B97XD with basis set BS6 show longer Co-X (X are the atoms coordinated with Co) bond lengths in  $\omega$ B97XD geometries than those in the TPSS geometries. Among these bonds, the difference of the Co-N bond lengths is the largest. For the singlet states of **1**, (iPrPNP)CoCl, (tBuPNP)CoCl, and (tBuPNP)CoH, the Co-N bonds in the  $\omega$ B97XD geometries are longer than those in the TPSS geometries by 0.056, 0.081, 0.077, and 0.058 Å, respectively. For the corresponding triplet states, these values become 0.121, 0.120, 0.113, and 0.168 Å, respectively, all larger.

Table S3: Free energies in toluene ( $\Delta G_{\text{toluene}}$  in kcal/mol) for (iPrPNP)CoCl, (tBuPNP)CoCl, and (tBuPNP)CoH.

	(iPrPNP)CoCl	(iPrPNP)CoCl T-Td
$\omega$ B97XD	0.0	-17.1
TPSS	0.0	-0.3
	(tBuPNP)CoCl	(tBuPNP)CoCl T-Td
$\omega$ B97XD	0.0	-6.5
TPSS	0.0	11.2
	(tBuPNP)CoH	(tBuPNP)CoH T-Td
$\omega$ B97XD	0.0	-0.9
TPSS	0.0	13.4

With TPSS, singlet and triplet states of selected stationary points involved in our proposed mechanism, especially three four-coordinate cobalt species (iPrPNP)CoBPin (**11** in Figure 1), (iPrPNP)CoPh (**16** in Figure 6), and (iPrPNP)CoH (**20** in Figure 6) were calculated. Geometries were optimized in gas phase by using the

basis set BS5 (this basis set was also used in Table 2 in the text), where Co uses 6-31+G\* and the others use 6-31G\*. Then the SMD single point calculations were conducted in benzene with Def2TZVP. The keyword “ultrafine” was used in these calculations. At the level of TPSS/Def2TZVP(SMD)//TPSS/BS5 with “ultrafine”, **1<sup>T</sup>.Td** is higher than **1** by 1.6 kcal/mol, which is close to the value of 2.2 kcal/mol at the level of TPSS/Def2TZVP(SMD)//TPSS/BS6 without “ultrafine”. Thus, optimized geometries at BS5 and BS6 are considered to be close to each other. Consistent with the crystal field splitting prediction that octahedral Co<sup>3+</sup> complexes adopt singlet ground states, the triplet state of complex **2<sup>T</sup>** could not be located, where the optimizations of the initial structure **2<sup>T</sup>** converge to the triplet **4<sup>T</sup>**. Similarly, optimizations of the initial structures **22<sup>T</sup>** and **23<sup>T</sup>** converge to the  $\sigma$ -complexes where the hydride on Co moves close to the BPin group to form a  $\sigma$ -bond coordinated H-BPin substituent. According to the results in Table S4, all the singlet states are lower than their corresponding triplet states by more than 6 kcal/mol. Thus, the results reported in the text are related to the singlet states.

Table S4: Comparisons of the free energies in benzene ( $\Delta G_{C_6H_6}$  in kcal/mol) for singlet and triplet states of selected stationary points at the level of TPSS/Def2TZVP(SMD)//TPSS/BS5. Corresponding singlet states are used as the energy reference.

0.0	15.8	
<b>4</b>	<b>4<sup>T</sup></b> (relative to <b>4</b> )	
<b>11</b>	<b>11<sup>T</sup></b> (relative to <b>11</b> )	<b>11<sup>T</sup>.Td</b> (relative to <b>11</b> )
0.0	6.4	
0.0	15.2	13.5
<b>5</b>	<b>5<sup>T</sup></b> (relative to <b>5</b> )	
<b>16</b>	<b>16<sup>T</sup></b> (relative to <b>16</b> )	<b>16<sup>T</sup>.Td</b> (relative to <b>16</b> )
0.0	26.5	
0.0	14.6	8.9
<b>TS<sub>8-9</sub></b>	<b>TS<sub>8-9</sub><sup>T</sup></b> (relative to <b>TS<sub>8-9</sub></b> )	<b>TS<sub>7-8</sub><sup>T</sup></b> (relative to <b>TS<sub>8-9</sub></b> )
<b>20</b>	<b>11<sup>T</sup></b> (relative to <b>20</b> )	<b>11<sup>T</sup>.Td</b> (relative to <b>20</b> )
0.0	8.3	12.2 <sup>1</sup>
0.0	16.0	12.4
<b>9</b>	<b>9<sup>T</sup></b> (relative to <b>9</b> )	
<b>22</b>	<b>22<sup>T</sup></b> (relative to <b>22</b> )	
0.0	9.7	
0.0	17.7	
<b>TS<sub>9-10</sub></b>	<b>TS<sub>9-10</sub><sup>T</sup></b> (relative to <b>TS<sub>9-10</sub></b> )	
<b>23</b>	<b>23<sup>T</sup></b> (relative to <b>23</b> )	

0.0	17.4	
-----	------	--

<sup>1</sup> the corresponding singlet state **TS**<sub>7-8</sub> could not be located, so the value is relative to the singlet state **TS**<sub>8-9</sub>.

## SI2. Optimized geometries of some species involved in Figure 2

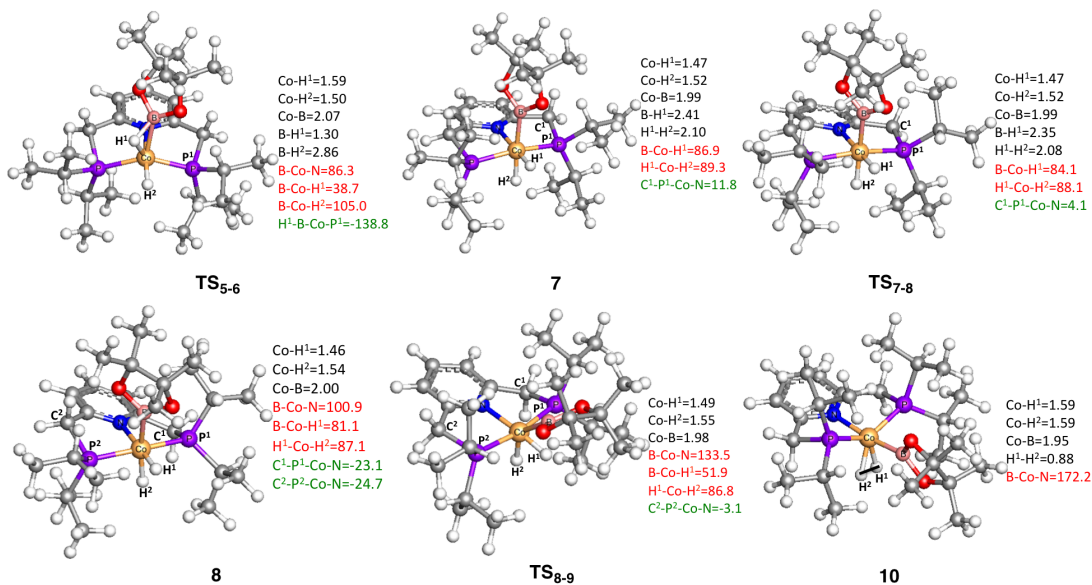
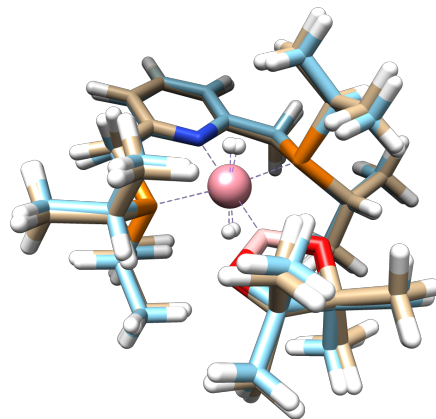


Figure S1: Optimized geometries of the species involved in Figure 2 but not shown in Figure 3. Some bond distances in Å, angles in °, and dihedral angles in ° are given in black, red, and green colors, respectively.

## SI3. The superimposed structures of the optimized geometry of 2 and its X-ray crystal structure



## SI4. An alternative pathway for the formation of 4 from 2

In addition to the path shown in Figure 2 in the text, an alternative pathway for the formation of **4** from **2** is shown in Figure S2. In this path, the two H atoms on Co in **2** firstly move towards BPin simultaneously via **2-4-TS1** with a very low barrier, generating an intermediate **2-4-Int1**. Subsequently, the five-membered phosphine ring in blue of **2-4-Int1** tips up to form **4** via transition state **2-4-TS2**. The stepwise pathway in which the two H atoms move towards BPin separately is unlikely, as optimizations of the structures generated by moving one H atom first repeatedly converge to **2**. The barrier for **2-4-TS1** is a little lower than that for **TS<sub>2-3</sub>** in Figure 2 in the text, while **2-4-Int1** and **2-4-TS2** are higher than **3** and **TS<sub>3-4</sub>**, respectively. However, the two pathways are considered to compete with each other, as the barrier for **2-4-TS2** is higher than that for **TS<sub>3-4</sub>** by only 1.3 kcal/mol.

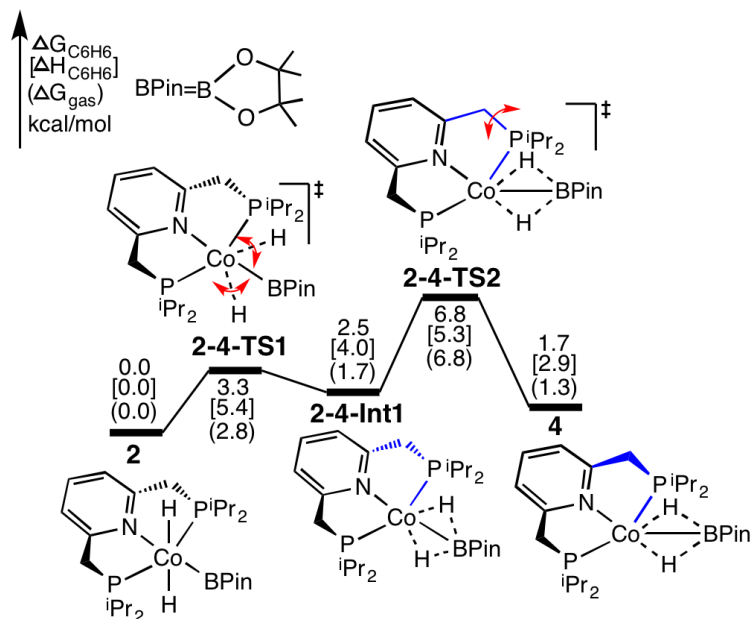


Figure S2: Calculated energy profiles for an alternative pathway for the formation of **4** from **2**.

## SI5. Formation of the isomer of 9

Possible pathways for the formation of the isomer of **9**, i.e., **9<sup>iso</sup>**, are shown in Figure S3. **9<sup>iso</sup>** adopts an octahedral geometry in which the two H atoms on Co and two phosphine ligands occupy the equatorial positions, and the pyridine and BPin occupy the axial positions. According to Figure S3, from the cobalt H<sub>2</sub>-complex **10**, H<sub>2</sub> can be cleaved through transition state **10-9<sup>iso</sup>-TS** in which the splitting two H atoms is moving towards the two phosphine ligands, respectively. The barrier for **10-9<sup>iso</sup>-TS** is very low, only 0.6 kcal/mol relative to **10**. The formed **9<sup>iso</sup>** is unstable, and is considered to overcome a barrier of only 1.1 kcal/mol for **10-9<sup>iso</sup>-TS** to regenerate **10**, which then releases H<sub>2</sub> to form **11**. In addition, **9<sup>iso</sup>** can also be formed from **9** via transition state **9-9<sup>iso</sup>-TS** that corresponds to the rotation of both BPin and two H atoms. However, this possibility is less favorable due to the high barrier of **9-9<sup>iso</sup>-TS**.

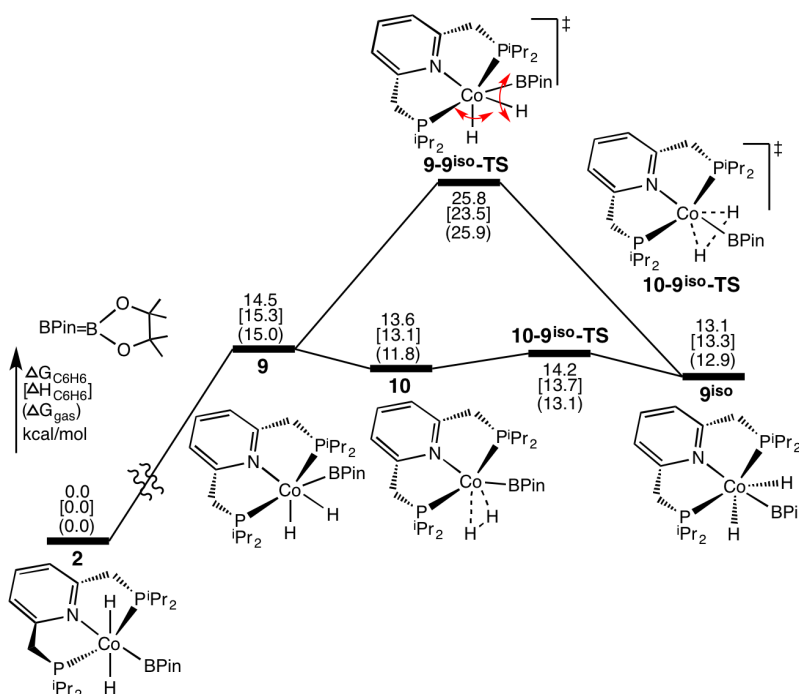


Figure S3: Calculated energy profiles for the formation of the isomer of **9**.

## SI6. Isomerization of **4** to its isomer

Fully optimizations of the structure that is generated along the backward direction of the imaginary frequency of **TS<sub>4-5</sub>** converge to **4'**, an isomer of **4**. The differences

between **4** and **4'** are the orientations of two *i*Pr groups on the phosphine ligands. Calculated energy profiles for the isomerizations of **4** to its isomers **4'** were shown in Figure S4. In this path, the *i*Pr group in blue firstly rotates through transition state **4-4'-TS1** to form intermediate **4-4'-Int1**, followed by the rotation of the other *i*Pr group in black through transition state **4-4'-TS2** to form **4'**. The barriers for the two transition states (**4-4'-TS1** and **4-4'-TS2**) are lower than that for **TS<sub>4-5</sub>** by a few kcal/mol. Thus, the isomerization process of **4** to its isomer **4'** via the rotation of *i*Pr groups is considered to occur very easily.

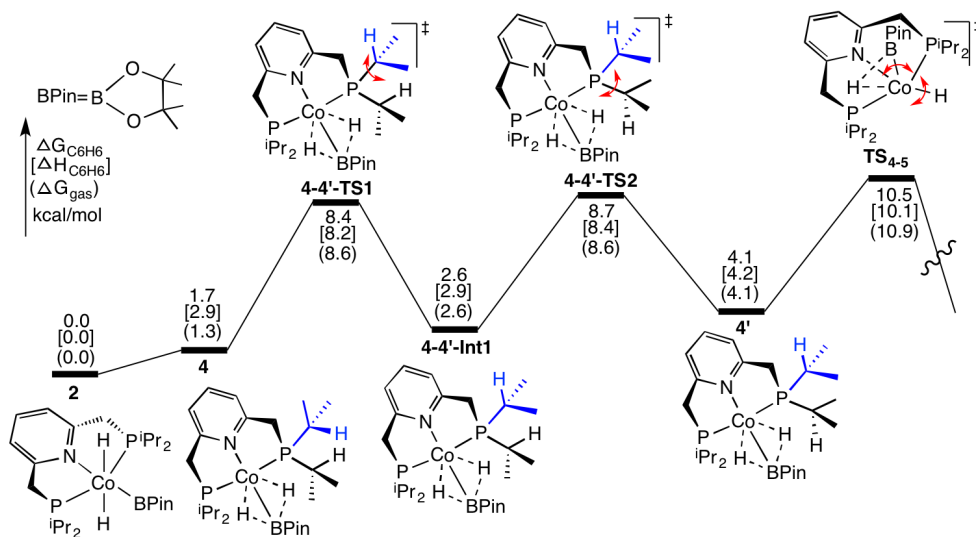


Figure S4: Calculated energy profiles for the isomerization of **4** to its isomer **4'**.

## SI7. Results for the release of H<sub>2</sub> from the *trans*-dihydride Co-complex with model systems

By using the calculation methods for the simplified systems, which have been described in Computational Details in the text, the mechanism for the release of H<sub>2</sub> from the *trans*-dihydride Co-complex with the model systems (i.e., *trans*-(<sup>Me</sup>PNP)CoH<sub>2</sub>(Beg) complex) was computed, and the calculated energy profiles are shown in Figure S5. The superscript “m” is added to the reported complexes related to the experimentally used systems to denote their corresponding model complexes. The mechanism shown in Figure S5 and S6 is similar to that for the experimentally used systems shown in Figure 2 in the text, which involves the formation of a *cis*-

dihydride Co-complex (i.e., *cis*-(<sup>Me</sup>PNP)CoH<sub>2</sub>(Beg) complex, **8<sup>m</sup>**) from *trans*-(<sup>Me</sup>PNP)CoH<sub>2</sub>(Beg) complex **2<sup>m</sup>** (Figure S5), followed by the release of H<sub>2</sub> from *cis*-(<sup>Me</sup>PNP)CoH<sub>2</sub>(Beg) complex, **8<sup>m</sup>** (Figure S6).

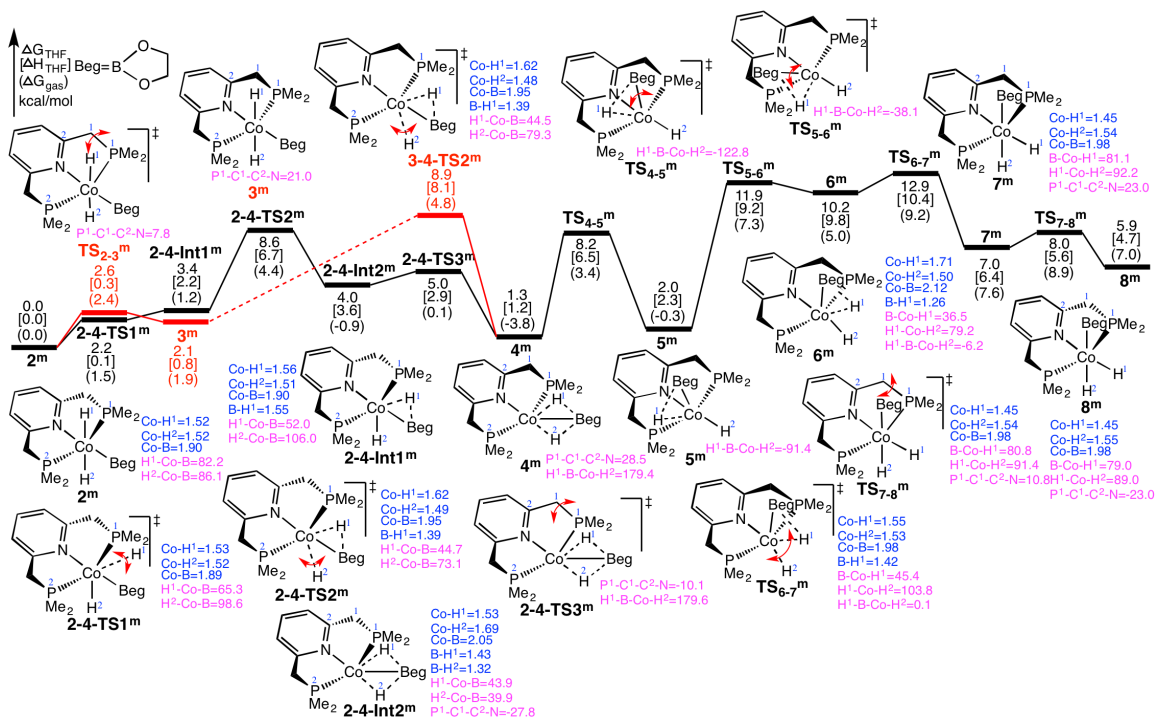


Figure S5: Calculated energy profiles for the formation of a *cis*-(<sup>Me</sup>PNP)CoH<sub>2</sub>(Beg) complex **8<sup>m</sup>** from *trans*-(<sup>Me</sup>PNP)CoH<sub>2</sub>(Beg) complex **2<sup>m</sup>**. Some bond lengths and angles are given in Å and °, respectively, and are next to their structures.

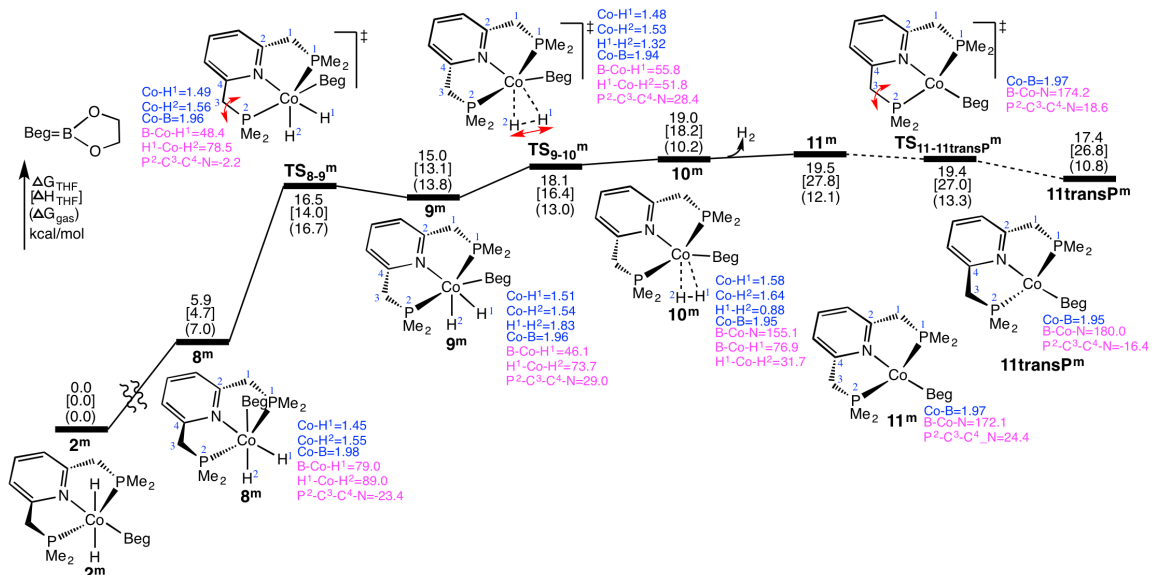


Figure S6: Calculated energy profiles for the release of H<sub>2</sub> from the *cis*-(<sup>Me</sup>PNP)CoH<sub>2</sub>(Beg) complex **2<sup>m</sup>**. Some bond lengths and angles are given in Å and °, respectively, and are next to their structures.

According to Figure S5, the two trans hydride atoms H<sup>1</sup> and H<sup>2</sup> in **2<sup>m</sup>** first move towards Beg in a stepwise way by crossing **2-4-TS1<sup>m</sup>** and **2-4-TS2<sup>m</sup>**, followed by the sp<sup>3</sup>-C<sup>1</sup> flipping transition state **2-4-TS3<sup>m</sup>**, giving an intermediate **4<sup>m</sup>** with two five-membered P ligands bending in the same direction. Optimizations of the concerted transition states by moving two H atoms simultaneously repeatedly converge to either **2-4-TS1<sup>m</sup>** or **2-4-TS2<sup>m</sup>**. Alternative to this pathway, another path for the formation of **4<sup>m</sup>** from **2<sup>m</sup>** via a process similar to that for the experimentally reported systems (see Figure 2 in the text) were calculated. In this path, the sp<sup>3</sup>-C<sup>1</sup> first flips through transition state **TS<sub>2-3</sub><sup>m</sup>** to form intermediate **3<sup>m</sup>**. However, the corresponding transition state **TS<sub>3-4</sub><sup>m</sup>** in which two hydride atoms move towards Beg simultaneously could not be located, and optimizations converge to a stepwise transition state **3-4-TS2<sup>m</sup>** for the movement of H<sup>2</sup>. Optimizations of the other transition state for the movement of H<sup>1</sup> and an intermediate between the two H-movement transition states repeatedly converge to either **3-4-TS2<sup>m</sup>** or **3<sup>m</sup>**. The barrier for **3-4-TS2<sup>m</sup>** is slightly higher than **2-4-TS2<sup>m</sup>**. Thus, this alternative path is less favorable than the path through **2-4-TS1<sup>m</sup>**, **2-4-TS2<sup>m</sup>**, and **2-4-TS3<sup>m</sup>**. From **4<sup>m</sup>**, the B-Co bond rotates anticlockwise via **TS<sub>4-5</sub><sup>m</sup>** to form a trigonal bipyramid complex **5<sup>m</sup>** where the H<sup>1</sup>-Beg and two P atoms are in the same plane. The B-Co bond further rotates anticlockwise via **TS<sub>5-6</sub><sup>m</sup>** to give intermediate **6<sup>m</sup>** in which H<sup>1</sup> and H<sup>2</sup> are *cis*. Subsequently, H<sup>1</sup> and H<sup>2</sup> atoms in **6<sup>m</sup>** rotate via **TS<sub>6-7</sub><sup>m</sup>**, followed by the sp<sup>3</sup>-C<sup>1</sup> flipping transition state **TS<sub>7-8</sub><sup>m</sup>** to generate the *cis*-dihydride cobalt-complex **8<sup>m</sup>**. The highest transition state for this process is **TS<sub>6-7</sub><sup>m</sup>** with a barrier of 12.9[10.4](9.2) kcal/mol relative to **2<sup>m</sup>**.

According to Figure S6, the sp<sup>3</sup>-C<sup>2</sup> of **8<sup>m</sup>** flips down via **TS<sub>8-9</sub><sup>m</sup>** to form **9<sup>m</sup>** with two P arm ligands bending in the same direction, followed by an H<sub>2</sub>-formation transition state **TS<sub>9-10</sub><sup>m</sup>** to form a dihydrogen cobalt complex **10<sup>m</sup>**. Complex **11<sup>m</sup>** is formed after releasing H<sub>2</sub>. In addition, the sp<sup>3</sup>-C<sup>2</sup> of **11<sup>m</sup>** could flip up via **TS<sub>11-11transP</sub><sup>m</sup>** to

form **11transP<sup>m</sup>** in which two five-membered phosphine rings are bent in different directions. The isomerization between **11<sup>m</sup>** and **11transP<sup>m</sup>** is considered to occur very easily, as the barriers for both directions are no more than 2 kcal/mol.

For the species involved in Figure S5 and S6, in **5<sup>m</sup>** and **6<sup>m</sup>**, two five-membered phosphine rings are bent in the same direction, and their isomers with two five-membered phosphine rings bending in different directions do not exist, as optimizations of the initial structures repeatedly converge to **5<sup>m</sup>** and **6<sup>m</sup>**, respectively. In addition, an isomer of **10<sup>m</sup>** in which two five-membered phosphine rings are bent in different directions is also unlikely, as optimizations of this isomer repeatedly converge to **10<sup>m</sup>**.

In addition to the pathways shown in Figure S5 and S6, a possible pathway for the formation of the cis-dihydride cobalt complex **8<sup>m</sup>** from the trans-dihydride cobalt complex **2<sup>m</sup>** via the dissociation and association of HBeg is shown in Figure S7. In this process, a transition state **TS<sub>2-4-int2-11\_transP<sup>m</sup></sub>** for the dissociation of HBeg was located, and was found to connect **2-4-Int2<sup>m</sup>** and **11\_transP<sup>m</sup>**. The barrier for the transition state **TS<sub>2-4-int2-11\_transP<sup>m</sup></sub>** is higher by 2.2[4.0] kcal/mol than that for **TS<sub>6-7<sup>m</sup></sub>** (the highest transition state in the formation of **8<sup>m</sup>** from **2<sup>m</sup>** through the path shown in Figure S5). Furthermore, the formation of **11\_transP<sup>m</sup>** and HBeg from **2<sup>m</sup>** is endothermic by 19.1 kcal/mol in enthalpy. Thus, this possible path is considered to be less favorable than that in Figure S5. In addition, an alternative pathway for the directly release of H<sub>2</sub> from the cis-dihydride cobalt complex **8<sup>m</sup>** through one transition state is calculated to be unlikely, as optimizations of the corresponding transition state repeatedly converge to **8<sup>m</sup>** again.

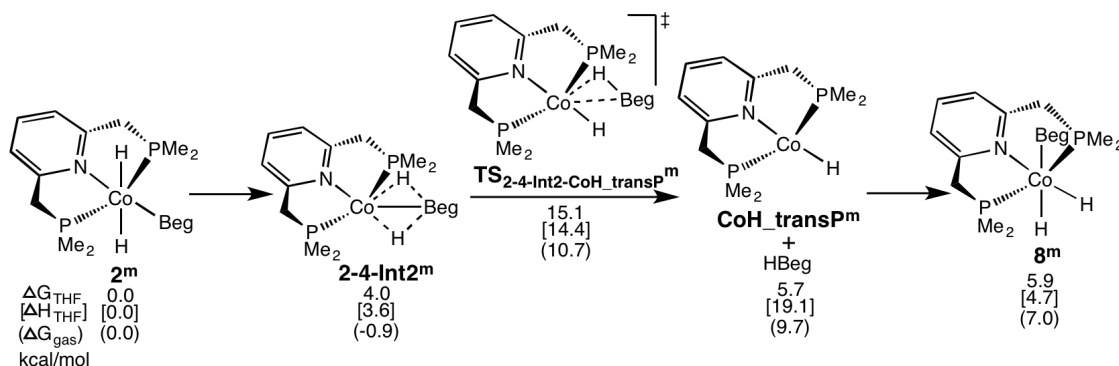


Figure S7: A possible pathway for the formation of the cis-dihydride cobalt complex **8<sup>m</sup>** from the trans-dihydride cobalt complex **2<sup>m</sup>** via the dissociation and association of HBeg. Values in kcal/mol are  $\Delta G_{\text{THF}}[\Delta H_{\text{THF}}](\Delta G_{\text{gas}})$ .

Another possible pathway for the formation of **8<sup>m</sup>** from **2<sup>m</sup>** through the dissociation of one phosphine ligand was also considered here. As shown in Figure S8, complex **2<sup>m</sup>\_openP** with one P arm ligand dissociated is very high in energy, 33.0[32.0](32.1) kcal/mol relative to **2<sup>m</sup>**. It should be noted that **2<sup>m</sup>\_openP** has a small imaginary frequency of  $-17.2 \text{ cm}^{-1}$ , while it is found to be a global minima with a keyword “ultrafine”. The scan results by freezing the dihedral angle  $\text{P}^2\text{C}^3\text{C}^4\text{N}$  shown in Figure S8 imply that there are no transition states for this process. As shown in Figure S8, the SCF energies of points 2-9 are over 30 kcal/mol relative to point 1 (point 1 is complex **2<sup>m</sup>**). Moreover, optimizations of points 5 and 6 converge to **2<sup>m</sup>** and **2<sup>m</sup>\_openP** respectively. Therefore, this possible pathway is less favorable than that in Figure S5.

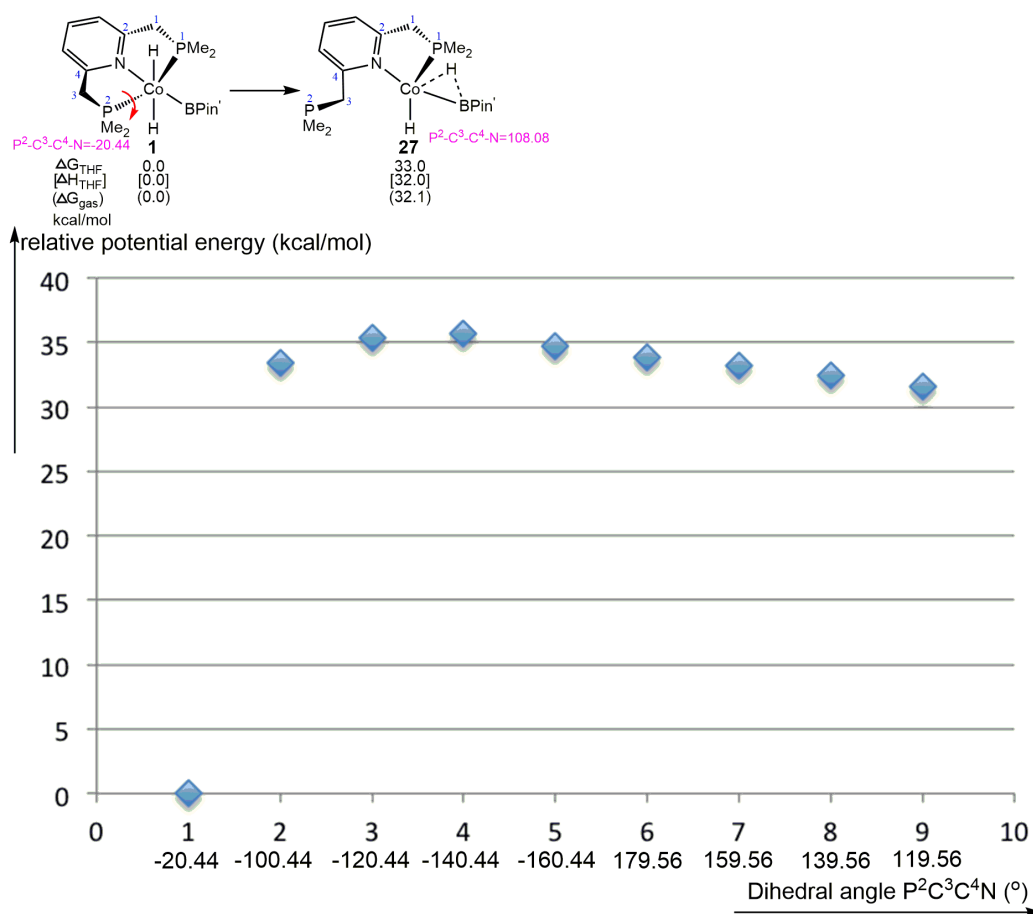


Figure S8: (A) Dissociation of one P arm ligand in **2<sup>m</sup>**; (B) Scan results for the dissociation of the P arm ligand in **2<sup>m</sup>**.

Milstein and coworkers have synthesized a series of PNP pincer ligated metal complexes that are similar to the trans-dihydride Co-complex in this study. The complexes reported by Milstein and coworkers are well known to show a mode of metal-ligand cooperation based on the ligand's aromatization/dearomatization. Thus, a possible pathway for the release of H<sub>2</sub> via the dearomatization of the pyridine ligand was calculated and the results are shown in Figure S9. Relative to **2<sup>m</sup>**, the barrier for the H<sub>2</sub> formation transition state **TS<sub>2-12<sup>m</sup></sub>** is very high, 35.7[34.9](29.6) kcal/mol. Thus, this possible pathway is also less favorable than that shown in Figure S5 and S6.

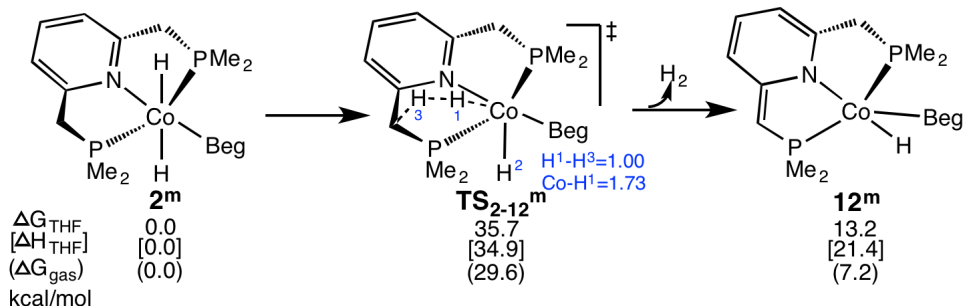


Figure S9: A possible pathway for the release of H<sub>2</sub> via the dearomatization of the pyridine ligand.

### SI8. Verification of $\omega$ B97XD/Def2TZVP(SMD)// $\omega$ B97XD/BS4

According to Figure S10, optimized geometry of complex **2** at the level of BS4 with  $\omega$ B97XD is close to its X-ray crystal structure. In addition, according to the results in Table S5, the free energies in gas phase at the levels of BS1 and BS4 with  $\omega$ B97XD vary more than 5 kcal/mol, while the energy results in C<sub>6</sub>H<sub>6</sub> at the level of  $\omega$ B97XD/Def2TZVP by using the optimized geometries at BS1 and BS4 are close to each other with the variation less than 1 kcal/mol. Thus, the level of Def2TZVP/BS4 is reasonable in calculating this system by giving results close to that at the level of Def2TZVP/BS1.

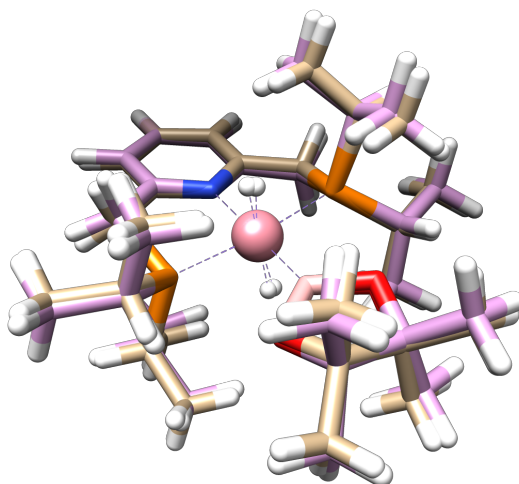


Figure S10: The superimposed structures of the X-ray crystal structure of complex **2** and its optimized geometry at the level of  $\omega$ B97XD/BS4.

Table S5: Results at the levels of  $\omega$ B97XD/Def2TZVP(SMD)// $\omega$ B97XD/BS1 and  $\omega$ B97XD/Def2TZVP(SMD)// $\omega$ B97XD/BS4. Values in kcal/mol are  $\Delta G_{C6H6}[\Delta H_{C6H6}](\Delta G_{gas})$ .

	<b>2</b>	<b>TS<sub>9-10</sub></b>	<b>11 + H<sub>2</sub></b>
$\omega$ B97XD/Def2TZVP(SMD) // $\omega$ B97XD/BS1	0.0[0.0](0.0)	18.5[19.8](17.6)	11.3[21.4](9.9)
$\omega$ B97XD/Def2TZVP(SMD) // $\omega$ B97XD/BS4	0.0[0.0](0.0)	18.2[19.5](17.2)	10.7[21.3](4.8)

### S19. Optimized geometries of transition states for the release of H<sub>2</sub> from **2<sup>Ir</sup>**, **2<sup>Ph</sup>**, **2<sup>Ir-Ph</sup>**, and **2<sup>Ir-Ph-tBu</sup>**

Pathways for the release of H<sub>2</sub> from **2<sup>R</sup>** (R= Ir, Ph, Ir\_Ph, and Ir\_Ph\_tBu) were calculated at the level of  $\omega$ B97XD/Def2TZVP(SMD)// $\omega$ B97XD/BS4. Optimized geometries of corresponding transition states (**TS<sub>9-10<sup>R</sup></sub>** and **TS<sub>2-12<sup>R</sup></sub>**) at the level of  $\omega$ B97XD/BS4 in gas phase are shown in Figure S11.

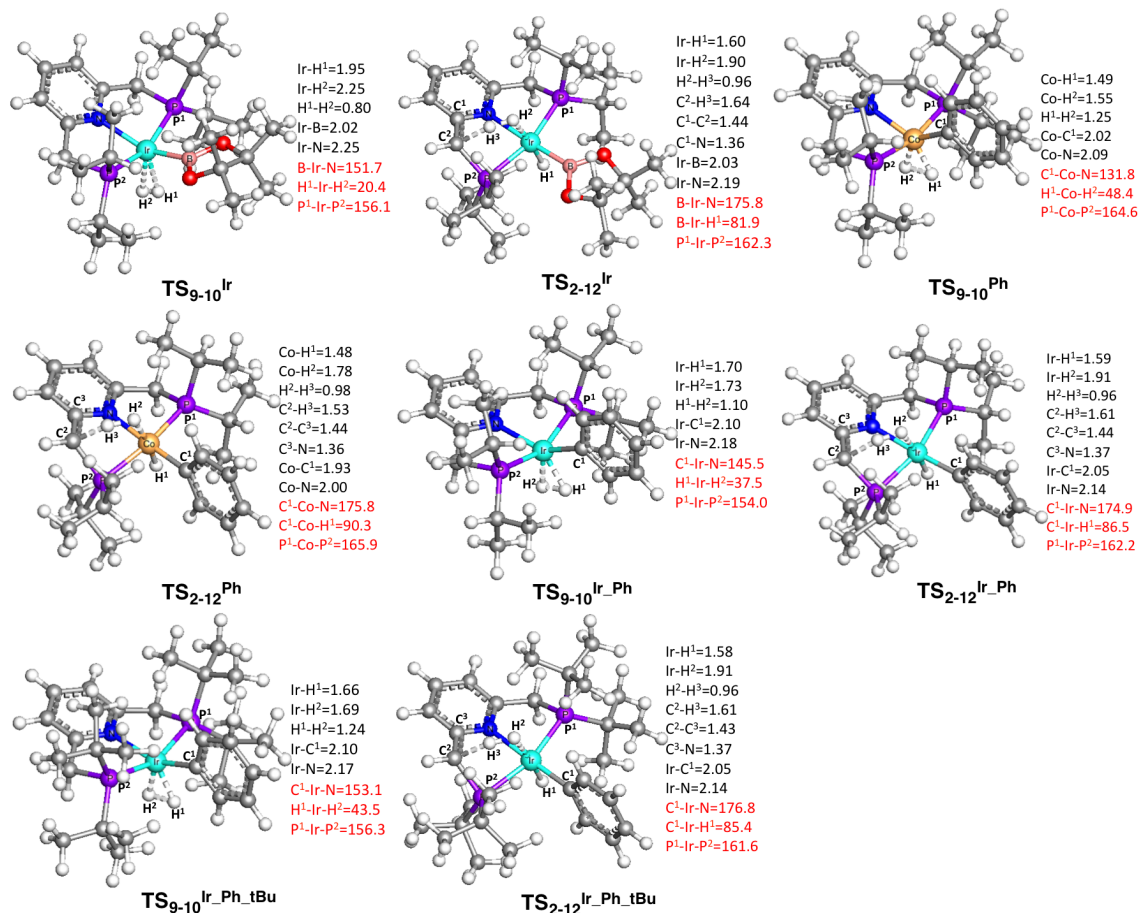


Figure S11: Optimized geometries of transition states (TS<sub>9-10</sub><sup>R</sup> and TS<sub>2-12</sub><sup>R</sup>) for the release of H<sub>2</sub> from 2<sup>R</sup> (R= Ir, Ph, Ir\_Ph, and Ir\_Ph\_tBu). Some bond distances in Å and angles in ° are given in black and red colors, respectively.

## SI10. A possible pathway for the formation of the active species from the catalyst precursor with model systems

Using the model systems, a possible pathway for the formation of the active species (<sup>Me</sup>PNP)CoBeg (**11<sup>m</sup>**) from the catalyst precursor (<sup>Me</sup>PNP)Co(CH<sub>2</sub>SiMe<sub>3</sub>) (**1<sup>m</sup>**) with the release of Me<sub>3</sub>SiCH<sub>2</sub>Beg is shown in Figure S12. The B-B bond of B<sub>2</sub>eg<sub>2</sub> is firstly cleaved via an oxidative addition transition state **1-11-TS1<sup>m</sup>** to form a Co(III) complex **1-11-Int<sup>m</sup>**, followed by the B-C elimination transition state **1-11-TS2<sup>m</sup>** to generate the active species **11<sup>m</sup>** with the release of Me<sub>3</sub>SiCH<sub>2</sub>Beg. This process is very favorable in thermodynamics. The B-B bond cleavage is the rate-determining

step with the barrier of 21.9 kcal/mol in free energy for **1-11-TS1<sup>m</sup>**. However, it is only 3.2 kcal/mol in enthalpy. Taking into account that the free energies are usually overestimated, the barrier of **1-11-TS1<sup>m</sup>** is considered to be accessible under the experimental conditions.

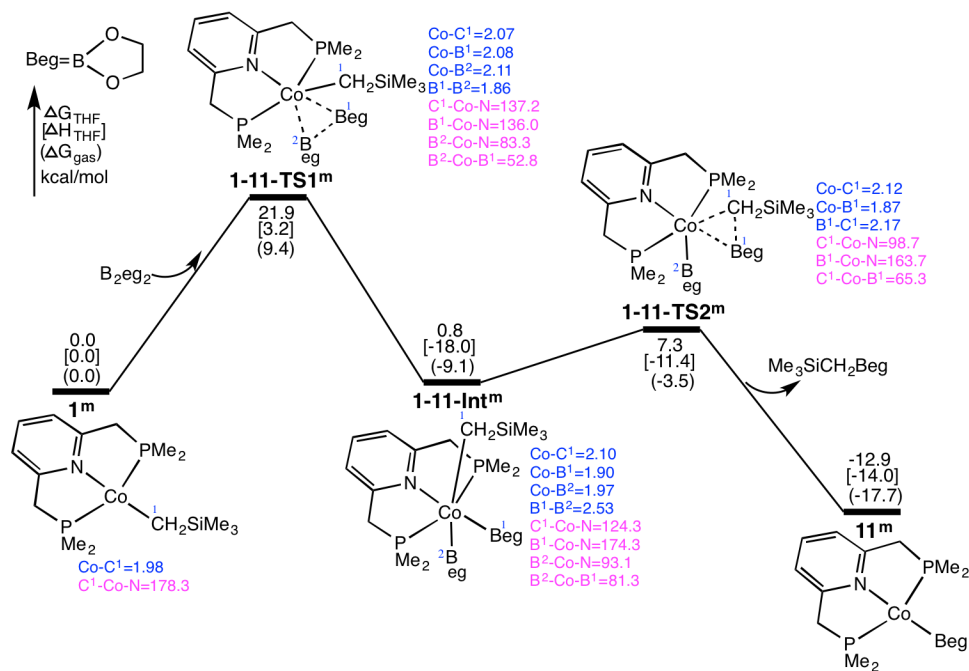


Figure S12: Calculated energy profiles for the formation of the active species ( $\text{MePNP}$ )CoBeg (**11<sup>m</sup>**) from the catalyst precursor ( $\text{MePNP}$ )Co( $\text{CH}_2\text{SiMe}_3$ ) (**1<sup>m</sup>**) with the release of  $\text{Me}_3\text{SiCH}_2\text{Beg}$ .

## SI11. Alternative pathways for the addition of $\text{C}_6\text{H}_6$ to the cobalt boryl species with model systems

Using the model systems, several alternative pathways for the addition of  $\text{C}_6\text{H}_6$  to **11<sup>m</sup>** were investigated. For comparisons, the pathway shown in Figure 5 in the text was also calculated by using the model systems, and the energy profiles are shown in Figure S13 (A). Other alternative pathways are shown in Figure S13 (B), (C), and (D), respectively. The oxidative addition pathway via Figure S13 (B) leads to the formation of an isomer **13<sup>m</sup>** with distorted trigonal bipyramidal geometry (**13<sub>iso</sub><sup>m</sup>**) in which  $\text{C}_6\text{H}_5$  and Beg are switched. Oxidative addition pathways via Figure S13 (C)

and (D) directly generate **15<sup>m</sup>** with distorted octahedral geometry (see Figure S13) and its isomer (**15<sub>iso</sub><sup>m</sup>**) in which C<sub>6</sub>H<sub>5</sub> and H are switched. In details, C<sub>6</sub>H<sub>5</sub> and Beg are trans in **15<sup>m</sup>**, while C<sub>6</sub>H<sub>5</sub> and Beg are cis in **15<sub>iso</sub><sup>m</sup>**. Comparisons of these pathways in Figure S13 show that alternative pathways via (B), (C), and (D) are less favorable than the pathway via (A). In addition, possible  $\sigma$ -bond metathesis pathways are unlikely, as optimizations of corresponding metathesis transition states repeatedly converge to the transition states shown in Figure S13. Furthermore, another possible pathway for the oxidative addition of C<sub>6</sub>H<sub>6</sub> to the cobalt complex with one phosphine ligand dissociated can be excluded, as the transition state for this process (Figure S14) is calculated to be very high, 35.2[24.5](33.0) kcal/mol relative to separated **11** and C<sub>6</sub>H<sub>6</sub>.

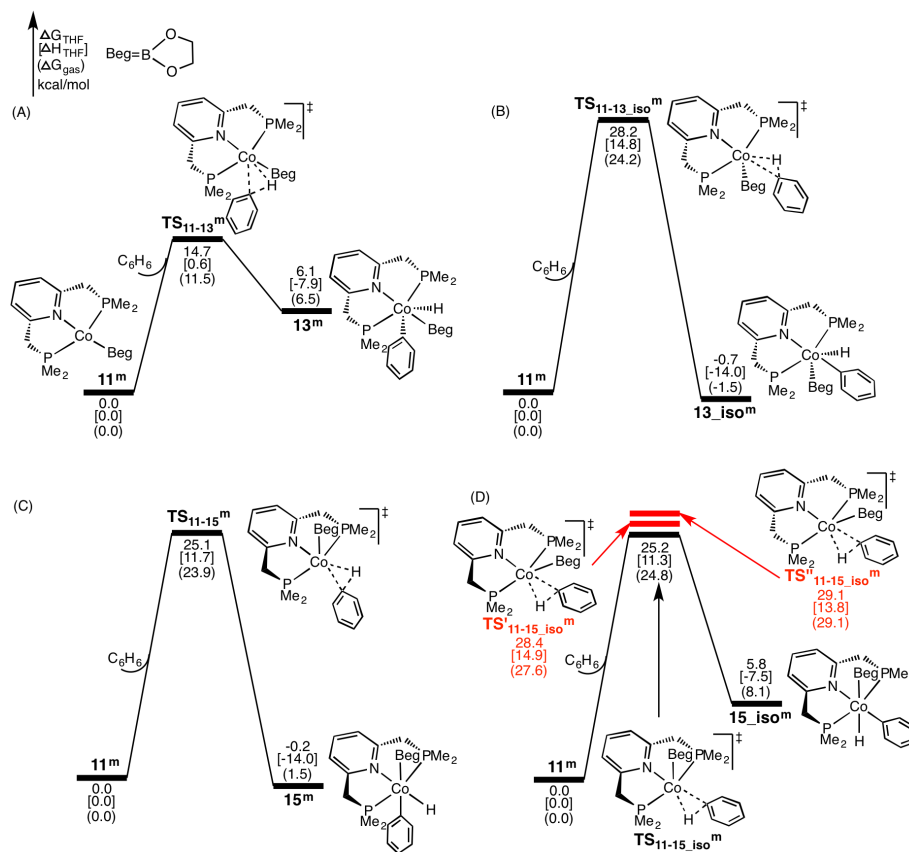


Figure S13: Calculated energy profiles for the addition of C<sub>6</sub>H<sub>6</sub> to **11<sup>m</sup>** via the pathway shown in Figure 5 in the text (A), via the pathway to form an isomer **13<sub>iso</sub><sup>m</sup>** (B), and via the pathway to form **15<sup>m</sup>** (C) and its isomer **15<sub>iso</sub><sup>m</sup>** (D). Values in kcal/mol are  $\Delta G_{\text{THF}}[\Delta H_{\text{THF}}](\Delta G_{\text{gas}})$ .

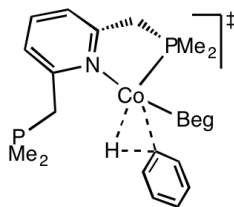


Figure S14: Structure of the transition state for the oxidative addition of  $C_6H_6$  to the Co species with one phosphine ligand dissociated.

## SI12. Comparisons of transition state $TS_{11-13}$ and that for the formation of **15** and its isomer

Like that for the model systems, alternative  $\sigma$ -bond metathesis pathways are still unlikely, as optimizations of possible metathesis transition states by using the experimentally reported systems repeatedly converge to the oxidative addition transition states. On the basis of the transition states  $TS_{11-15}^m$  and  $TS_{11-15\_iso}^m$ , corresponding transition states  $TS_{11-15}$  and  $TS_{11-15\_iso}$  were calculated. Relative to separated **11** and  $C_6H_6$ , the barriers for  $TS_{11-15}$  and  $TS_{11-15\_iso}$  are 40.5[24.8](37.9) and 42.1[25.9](39.5) kcal/mol, respectively, which are much higher than the barrier of 24.2[8.4](21.7) kcal/mol for  $TS_{11-13}$  in Figure 5 in the text. Comparisons of their optimized geometries (Figure 5 in the text and Figure S15) show that the BPin substituents at Co are bent much farther from the trans position of pyridine ligands in  $TS_{11-15}$  and  $TS_{11-15\_iso}$  than that in  $TS_{11-13}$ . It should be noted that BPin is in the trans position of pyridine ligands in **11**. Thus, distortion/interaction analysis of the transition states ( $TS_{11-13}$ ,  $TS_{11-15}$  and  $TS_{11-15\_iso}$ ) is conducted at the level of  $\omega$ B97XD/BS1, and the results are shown in Table S6. As shown in Table S6, the distortion energy of the substrate  $C_6H_6$  correlates well with the C-H distance. According to their optimized geometries, as the C-H distance increases, the corresponding Co-H and Co-C distances decrease. Thus, the interaction energy is mainly contributed by the energy released by forming Co-H and Co-C bonds. In addition, the activation energy correlates well with the distortion energy of the

cobalt catalyst. Therefore, the high barriers of transition states **TS<sub>11-15</sub>** and **TS<sub>11-15\_</sub>** are due to the high distortion energies of the cobalt catalyst.

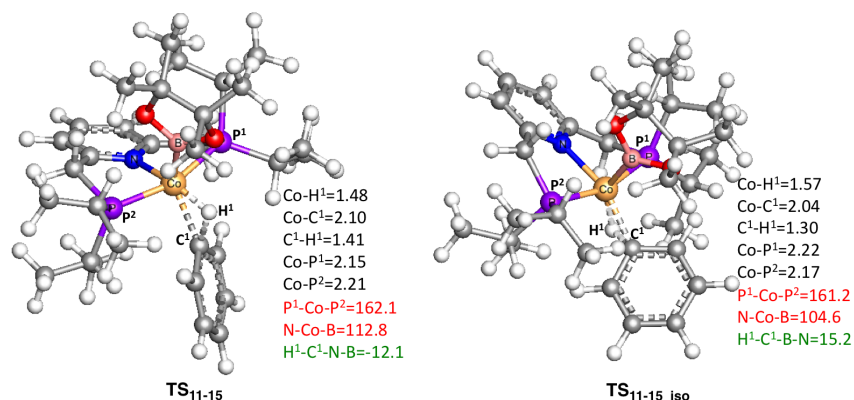


Figure S15: Optimized geometries of **TS<sub>11-15</sub>** and **TS<sub>11-15\_</sub>**. Some bond distances in Å, angles in °, and dihedral angles in ° are given in black, red, and green colors, respectively.

Table S6: Distortion/interaction analysis for the oxidative addition transition states **TS<sub>11-13</sub>**, **TS<sub>11-15</sub>** and **TS<sub>11-15\_</sub>** at the level of ωB97XD/BS1.

	$\Delta E^\ddagger$ (kcal/mol)	$\Delta E^\ddagger_{\text{dist}}$ (Co cat.) (kcal/mol)	$\Delta E^\ddagger_{\text{dist}}$ (C <sub>6</sub> H <sub>6</sub> ) (kcal/mol)	$\Delta E^\ddagger_{\text{int}}$ (kcal/mol)	C-H distance (Å)
<b>TS<sub>11-13</sub></b>	6.7	21.2	62.7	-77.3	1.60
<b>TS<sub>11-15</sub></b>	22.8	34.3	41.2	-52.7	1.41
<b>TS<sub>11-15_</sub></b>	23.8	38.1	26.1	-40.4	1.30

$\Delta E^\ddagger$  is the activation energy and is relative to separated **11** and C<sub>6</sub>H<sub>6</sub>;  $\Delta E^\ddagger_{\text{dist}}$  (Co cat.) and  $\Delta E^\ddagger_{\text{dist}}$  (C<sub>6</sub>H<sub>6</sub>) are the distortion energy of the cobalt catalyst and C<sub>6</sub>H<sub>6</sub>, respectively;  $\Delta E^\ddagger_{\text{int}}$  is the interaction energy.

### SI13. Addition of C<sub>6</sub>H<sub>6</sub> to corresponding Rh and Ir complexes

Possible pathways for the addition of C<sub>6</sub>H<sub>6</sub> to the corresponding Rh and Ir complexes were investigated by using their model complexes (**Rh11<sup>m</sup>** and **Ir11<sup>m</sup>**),

where all the *i*Pr substituents of the <sup>*i*</sup>PrPNP ligand were replaced with Me and B<sub>2</sub>Pin<sub>2</sub> was replaced with B<sub>2</sub>eg<sub>2</sub>. Thus, **Rh11<sup>m</sup>** and **Ir11<sup>m</sup>** are obtained by replacing Co in **11<sup>m</sup>** with Rh and Ir, respectively. The calculation methods employed here are similar to that used for the Co model systems, where Rh and Ir atoms use the same basis sets with that of Co. The  $\sigma$ -bond metathesis pathways for Rh and Ir complexes are unlikely, as optimizations of corresponding  $\sigma$ -bond metathesis transition states repeatedly converge to the oxidative addition transition states, which can be ascribed to the low oxidative state of Rh(I) and Ir(I) in **Rh11<sup>m</sup>** and **Ir11<sup>m</sup>**, respectively. According to the oxidative addition pathways for the Co complex shown in Figure S13 of SI11, pathway (A) via **TS<sub>11-13<sup>m</sup></sub>** is the most favorable one, followed by the pathways (C) and (D) for directly forming **15<sup>m</sup>** and its isomer via **TS<sub>11-15<sup>m</sup></sub>** and **TS<sub>11-15<sub>iso</sub><sup>m</sup></sub>**, respectively. Thus, these possible oxidative addition pathways for the corresponding Rh and Ir complexes were examined, and the results are shown in Table S7. For clarity, we added “Rh” and “Ir” in the front of Co complexes to represent their corresponding Rh and Ir complexes. Like the Co complex, the pathway via **RhTS<sub>11-13<sup>m</sup></sub>** and **IrTS<sub>11-13<sup>m</sup></sub>** is still more favorable than that for directly forming **Rh15<sup>m</sup>** and **Ir15<sup>m</sup>** and their isomers. Furthermore, the barriers for **RhTS<sub>11-13<sup>m</sup></sub>** and **IrTS<sub>11-13<sup>m</sup></sub>** are higher than that for **TS<sub>11-13<sup>m</sup></sub>**, which can be explained by the unfavorable conversion between Rh(I) and Rh(III), and that between Ir(I) and Ir(III).

Table S7: Results for oxidative addition transition states for Co, Rh, and Ir complexes by using the model systems. Values in kcal/mol are  $\Delta G_{\text{THF}}[\Delta H_{\text{THF}}](\Delta G_{\text{gas}})$ .

Co	<b>11<sup>m</sup></b> + C <sub>6</sub> H <sub>6</sub>	<b>TS<sub>11-13<sup>m</sup></sub></b>	<b>TS<sub>11-15<sup>m</sup></sub></b>	<b>TS<sub>11-15<sub>iso</sub><sup>m</sup></sub></b>
	0.0[0.0](0.0)	14.7[0.6](11.5)	25.1[11.7](23.9)	25.2[11.3](24.8)
Rh	<b>Rh11<sup>m</sup></b> + C <sub>6</sub> H <sub>6</sub>	<b>RhTS<sub>11-13<sup>m</sup></sub></b>	<b>RhTS<sub>11-15<sup>m</sup></sub></b>	<b>RhTS<sub>11-15<sub>iso</sub><sup>m</sup></sub></b>
	0.0[0.0](0.0)	26.7[12.9](23.3)	37.8[23.4](38.2)	38.9[25.0](40.8)
Ir	<b>Ir11<sup>m</sup></b> + C <sub>6</sub> H <sub>6</sub>	<b>IrTS<sub>11-13<sup>m</sup></sub></b>	<b>IrTS<sub>11-15<sup>m</sup></sub></b>	<b>IrTS<sub>11-15<sub>iso</sub><sup>m</sup></sub></b>
	0.0[0.0](0.0)	25.0[10.9](17.8)	35.9[22.3](32.7)	35.9[22.9](32.7)

## SI14. Optimized geometries for the species in Figure 6 in the text

Optimized geometries for the species involved in Figure 6 (the reductive elimination of B-C bond to form PhBPIn) in the text are shown in Figure S16.

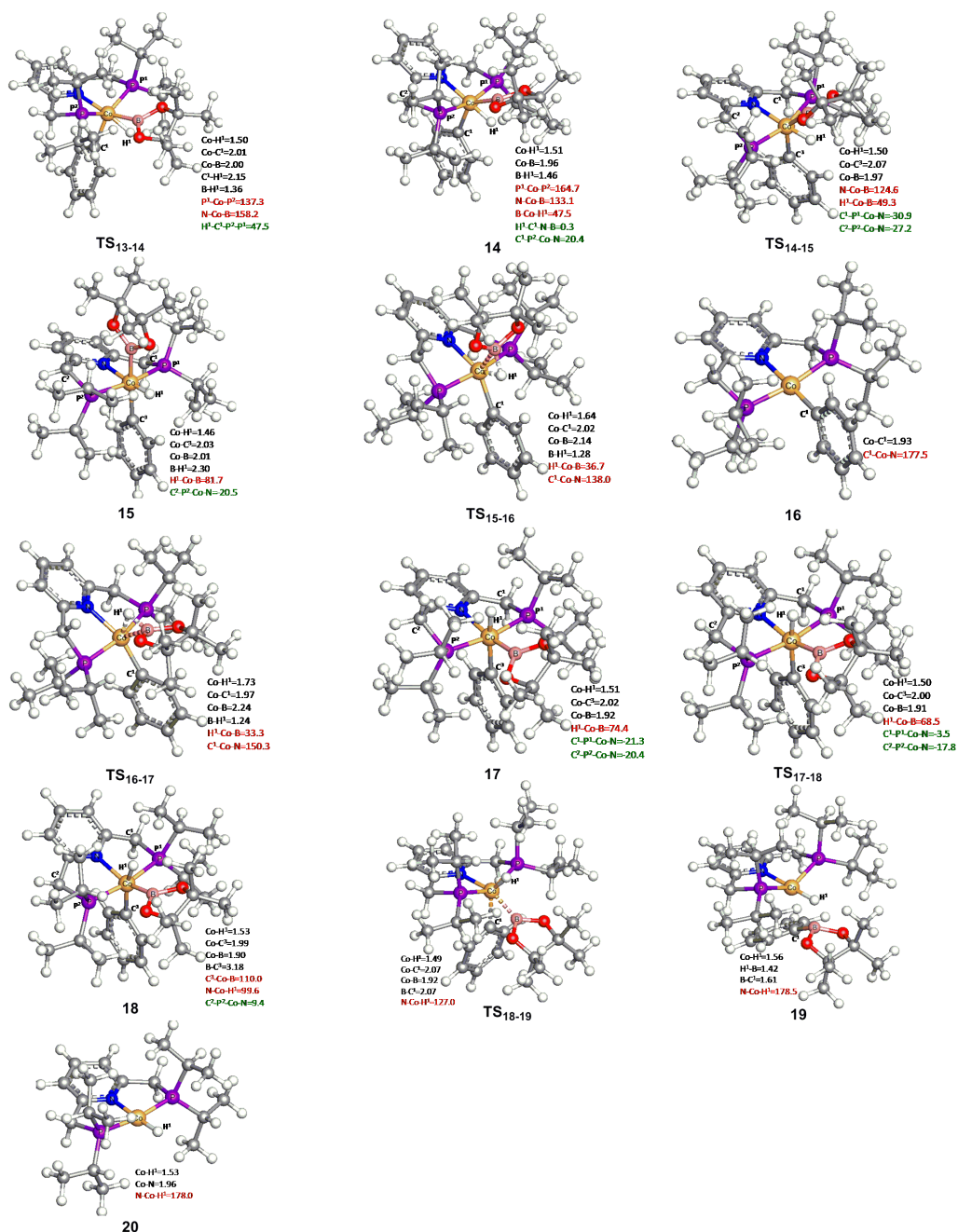


Figure S16: Optimized geometries of the species involved in Figure 6 in the text. Some bond distances in Å, angles in °, and dihedral angles in ° are given in black, red, and green colors, respectively.

## SI15. Results for the reductive elimination of the B-C bond with model systems

With model systems, calculated energy profiles for the reductive elimination of the B-C bond via the pathway similar with that in Figure 6 in the text are shown in Figure S17. It should be noted that the dissociation of HBeg from the Co(III) complex **15<sup>m</sup>** leads to the formation of **16<sub>cisP<sup>m</sup></sub>** where the two P arms are bent in the same direction. Similar to the results of the real catalyst in Figure 6 in the text, the formation of PhBeg from complex **13<sup>m</sup>** is also very favorable in thermodynamics. Comparisons of the transition states involved in Figure S17 show that the transition state **TS<sub>18-19<sup>m</sup></sub>** corresponding to the reductive elimination of the B-C bond is the highest one, and it is slightly lower by 0.5 kcal/mol than the C-H oxidative addition transition state **TS<sub>11-13<sup>m</sup></sub>** in Figure S13(A).

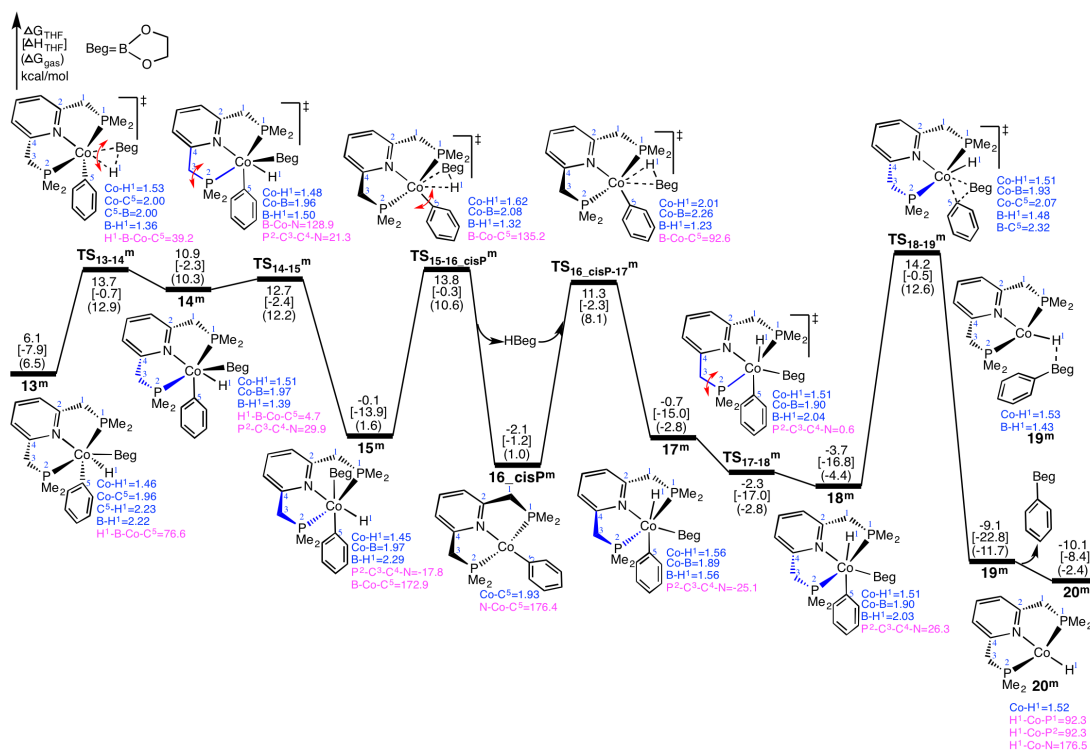


Figure S17: Calculated energy profiles for the reductive elimination of the B-C bond to generate the borylated product PhBeg by using model systems through the mechanism similar with that in Figure 6 in the text. The energies for these species are relative to separate  $C_6H_6$  and **11<sup>m</sup>**.

In addition to the mechanism shown in Figure S17, several other possibilities were considered, which includes the reductive elimination of the B-C bond through the direct reductive elimination from **13<sup>m</sup>** (Figure S18), through an isomer of transition state **TS<sub>18-19<sup>m</sup></sub>** where two phosphine ligands are bent in different directions (Figure S19(A)), through a transition state with the assist of HBeg (Figure S19(B)), through the reductive elimination from **15\_iso<sup>m</sup>** or its isomer where the cleaved C<sub>6</sub>H<sub>5</sub> and H are in cis positions (Figure S19(C)), and through the dissociation of one phosphine ligand from **13<sup>m</sup>** (Figure S19(D)). Furthermore, another pathway through the oxidative addition of B<sub>2</sub>eg<sub>2</sub> to **16\_transP<sup>m</sup>** and the following reductive elimination of the B-C bond was also considered (Figure S20). All these possible pathways are less favorable than that shown in Figure S17, as the corresponding transition states or intermediates are higher than the rate-determining transition state **TS<sub>18-19<sup>m</sup></sub>** in Figure S17. With the experimentally reported systems, the process for the reductive elimination of the B-C bond to generate the borylated product PhBPIn through the direct reductive elimination from **13** was further calculated to be unlikely, as the barrier for **TS<sub>13-20</sub>** is very high, 38.4[23.6](36.3) kcal/mol relative to separated C<sub>6</sub>H<sub>6</sub> and **11** (Figure S21). In addition, another possible pathway for the oxidative addition of C<sub>6</sub>H<sub>6</sub> to the Co(I) complex **20<sup>m</sup>** was also considered, while it is calculated to be less favorable both in thermodynamics and kinetics than the oxidative addition of B<sub>2</sub>eg<sub>2</sub> to regenerate the active species (Figure S24 in SI17).

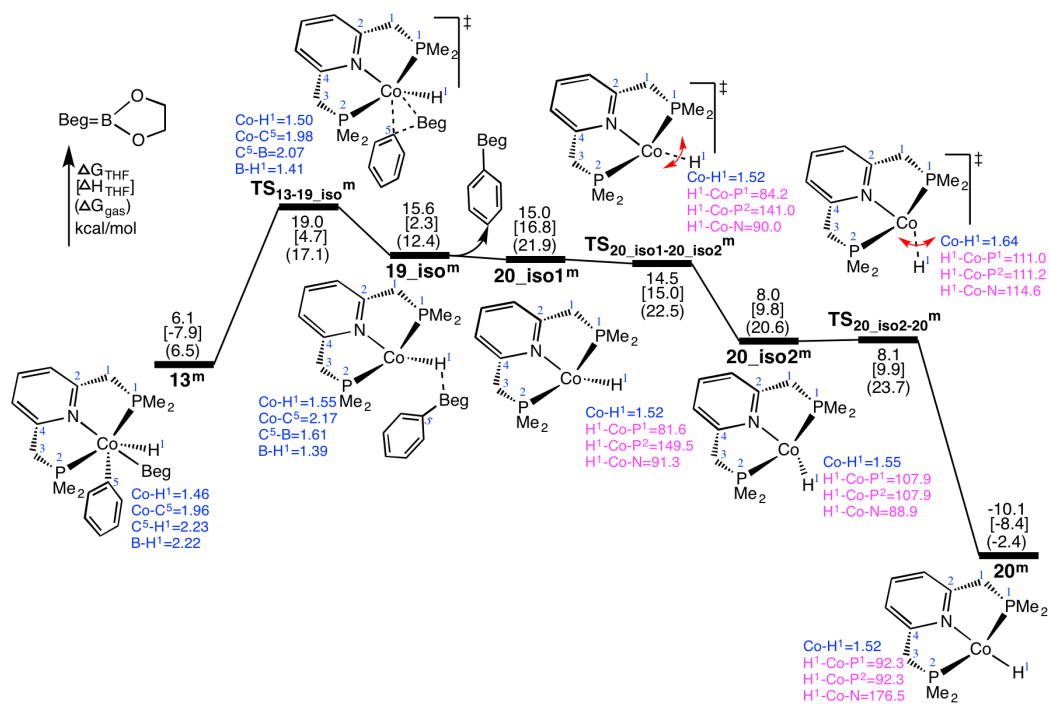


Figure S18: Calculated energy profiles for the reductive elimination of the B-C bond to generate the borylated product PhBeg by using model systems through the direct reductive elimination from **13<sup>m</sup>**. The energies for these species are relative to separate  $C_6H_6$  and **11<sup>m</sup>**.

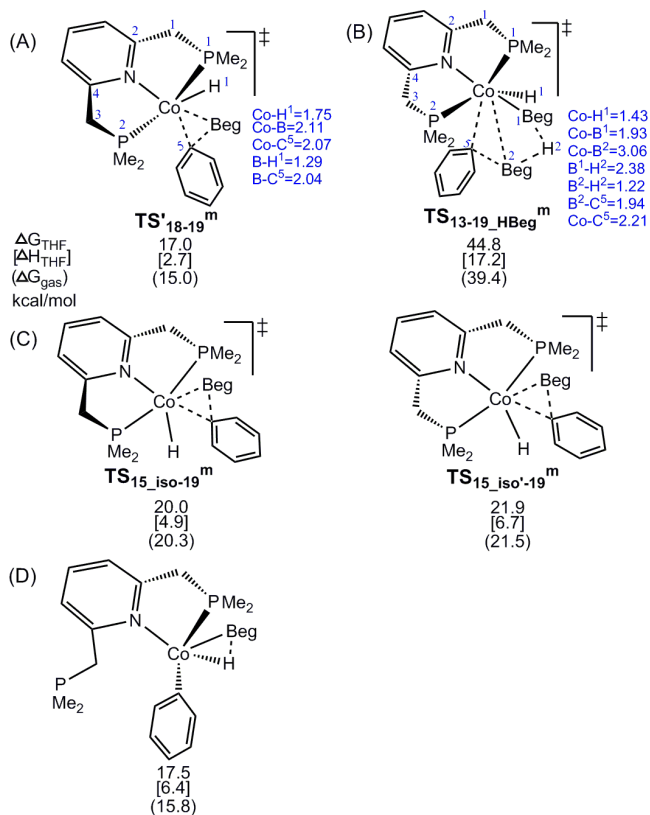


Figure S19: (A) An isomer of transition state  $\text{TS}_{18-19}$  where two phosphine ligands are bent in different directions; (B) a transition state for the reductive elimination of B-C bond with the assist of HBeg; (C) transition states for the reductive elimination of B-C bond from  $\mathbf{15\_iso}^m$  or its isomer; (D) an intermediate formed via the dissociation of one phosphine ligand from  $\mathbf{13}^m$ . The energies for  $\text{TS}_{13-19\_HBeg}^m$  are relative to separate  $\text{C}_6\text{H}_6$ , HBeg, and  $\mathbf{11}^m$ , and the energies for the others are relative to separate  $\text{C}_6\text{H}_6$  and  $\mathbf{11}^m$ .

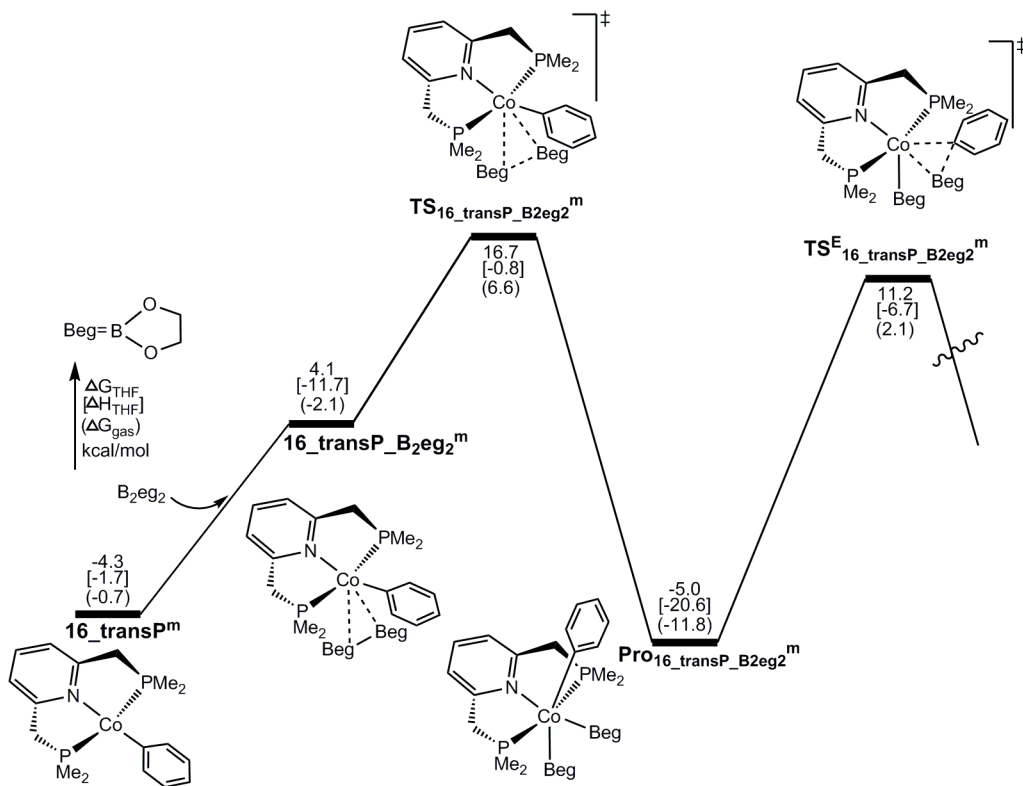


Figure S20: Calculated energy profiles for the oxidative addition of  $B_2eg_2$  to **16\_transP<sup>m</sup>** and the following reductive elimination of the B-C bond. The energies for these species are relative to separate  $C_6H_6$  and **11<sup>m</sup>**.

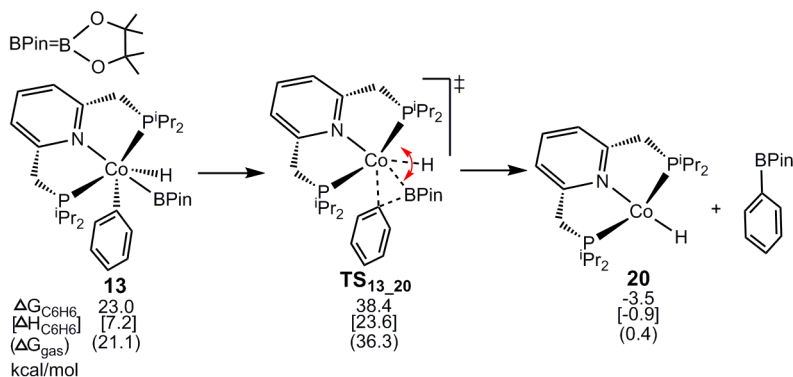


Figure S21: Calculated results for the reductive elimination of the B-C bond to generate the borylated product PhBPIn by using experimentally reported systems through the direct reductive elimination from **13**. The energies for these species are relative to separate  $C_6H_6$  and **11**.

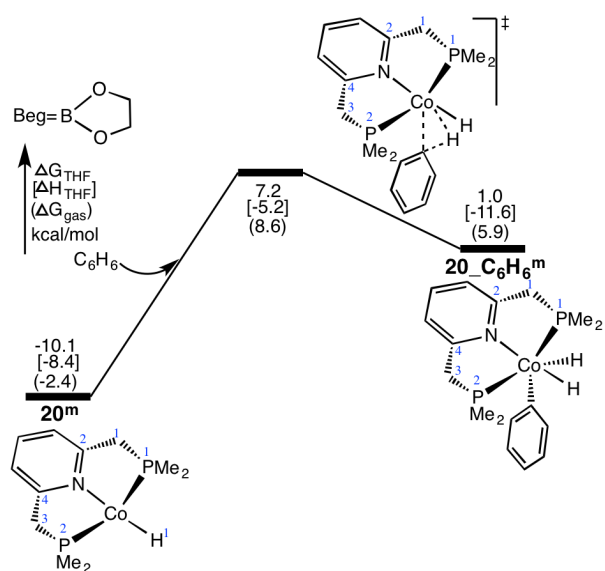


Figure S22: Calculated energy profiles for the oxidative addition of  $C_6H_6$  to  $20^m$ . The energies for these species are relative to separate  $C_6H_6$  and  $11^m$ .

### SI16. Optimized geometries of the species in Figure 7

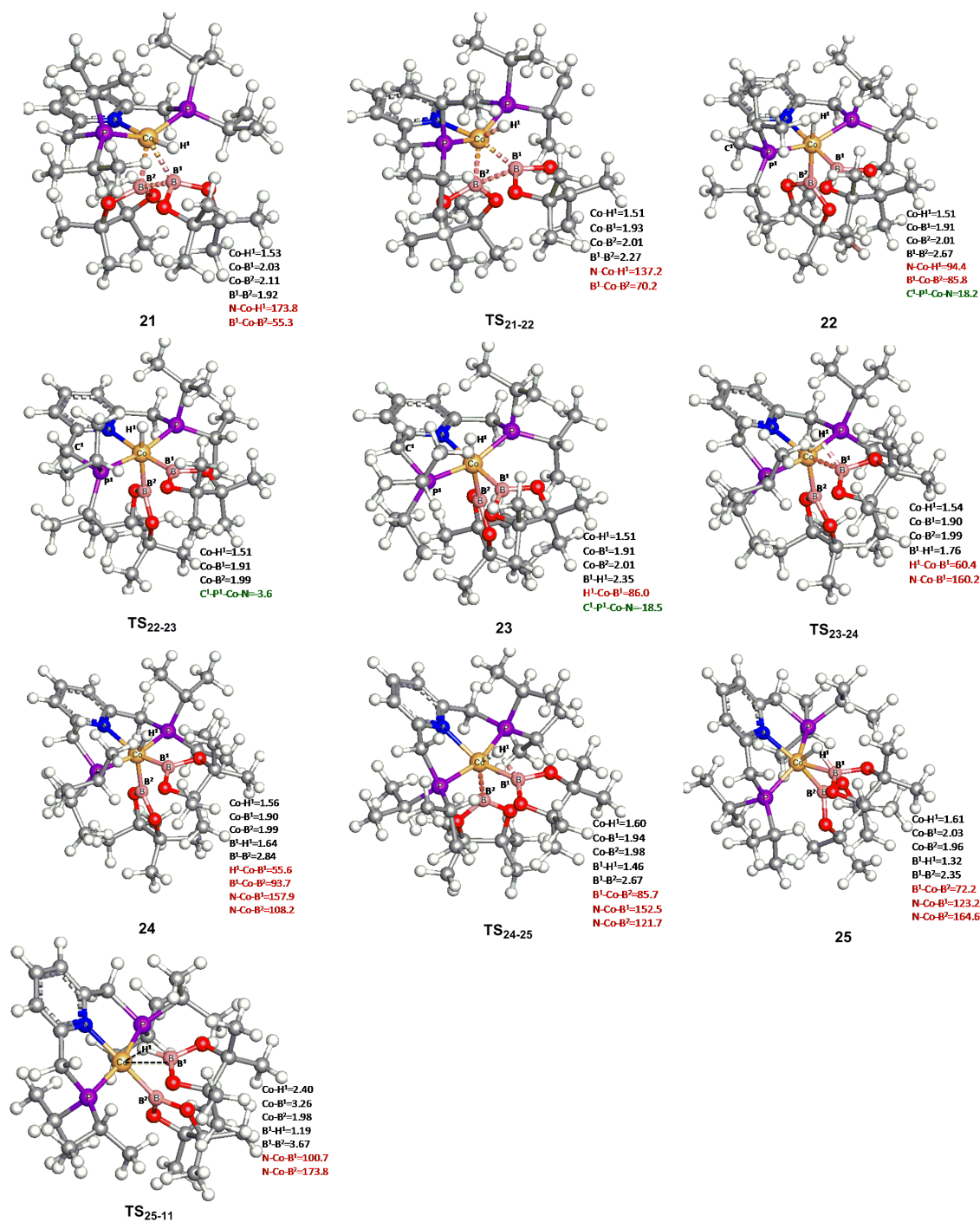


Figure S23: Optimized geometries of the species in Figure 7. Some bond distances and angles are given in Å and °, respectively.

## SI17. Results for the regeneration of the active species with model systems

Using the model systems ( $(^{\text{Me}}\text{PNP})\text{CoH}$  (**20<sup>m</sup>**) and  $\text{B}_2\text{eg}_2$ ), the pathways for the regeneration of  $(^{\text{Me}}\text{PNP})\text{CoBeg}$  (**11<sup>m</sup>**) from  $(^{\text{Me}}\text{PNP})\text{CoH}$  (**20<sup>m</sup>**) and  $\text{B}_2\text{eg}_2$  were calculated by following the similar mechanism with that in Figure 7 in the text. Consistent with the real catalyst systems in Figure 7, the process for the formation of **11<sup>m</sup>** and  $\text{HBeg}$  from **20<sup>m</sup>** and  $\text{B}_2\text{eg}_2$  is also favorable in both thermodynamics and kinetics (Figure S24).

In **21<sup>m</sup>**, the B-B bond is in parallel with the line of N-Co-H. An isomer of **21<sup>m</sup>** in which the B-B bond is in parallel with the line of P-Co-P is  $-3.5[-3.4](1.7)$  kcal/mol relative to **21<sup>m</sup>**. However, this isomer could not lead the reaction to generate **11<sup>m</sup>**. Instead, this isomer can be considered to dissociate  $\text{B}_2\text{eg}_2$  to regenerate **20<sup>m</sup>**, which then associates with  $\text{B}_2\text{eg}_2$  to form **21<sup>m</sup>** again.

In addition to the pathway for the formation of **24<sup>m</sup>** from **22<sup>m</sup>** via **23<sup>m</sup>**, an alternative pathway through **22-24-Int<sup>m</sup>** (the path in red) was also considered. In this path, the H and Beg on Co firstly move towards each other via **22-24-TS1<sup>m</sup>** to form complex **22-24-Int<sup>m</sup>**, followed by another transition state **22-24-TS2<sup>m</sup>** for the  $\text{sp}^3\text{-C}$  of one phosphine ring flipping up to give complex **24<sup>m</sup>**. Although the transition state **TS<sub>23-24<sup>m</sup></sub>** in the black pathway was not successfully located, the path in red is predicted to be less favorable than the path in black, as the barrier for **22-24-TS2<sup>m</sup>** is calculated to be higher than that for **TS<sub>22-23<sup>m</sup></sub>** and **TS<sub>23-24<sup>m</sup></sub>** by  $3.3[3.1](1.4)$  and  $3.4[2.9](2.5)$  kcal/mol, respectively, at the level of  $\omega\text{B97XD}/\text{BS3}(\text{SMD}, \text{THF})//\omega\text{B97XD}/\text{BS4}$ . In this level, geometries were optimized in gas phase at the level of  $\omega\text{B97XD}/\text{BS4}$  in which LANL2DZ is used for Co and 6-31G\* for the others, and the single point solvent corrections were then conducted in THF with the SMD model at the level of  $\omega\text{B97XD}/\text{BS3}$  where the SDD ECP-basis set is used for Co and cc-pVTZ for the others, which is similar to the methods for the single point solvent corrections described in Computational methods.

Furthermore, an alternative pathway for the formation of **25<sup>m</sup>** from **24<sup>m</sup>** in which the  $\text{sp}^3\text{-C}$  of one phosphine ring firstly flips up to generate an intermediate with two

phosphine rings bending in the same direction is unlikely, as optimizations of this corresponding intermediate in which two phosphine rings bend in the same direction repeatedly converge to **25<sup>m</sup>**.

The transition state **TS<sub>25-11<sup>m</sup></sub>** for the dissociation of HBeg from **25<sup>m</sup>** could not be located, while an alternative pathway in which the sp<sup>3</sup>-C of one phosphine ring firstly flips up via **25-11-TS1<sup>m</sup>** to form an intermediate **25-11-Int<sup>m</sup>**, followed by the dissociation of HBeg via **25-11-TS2<sup>m</sup>** to generate **11<sup>m</sup>** was calculated and shown in blue. According to the discussions in the text, this alternative pathway (in blue) is proposed to be slightly less favorable than that via **TS<sub>25-11<sup>m</sup></sub>**.

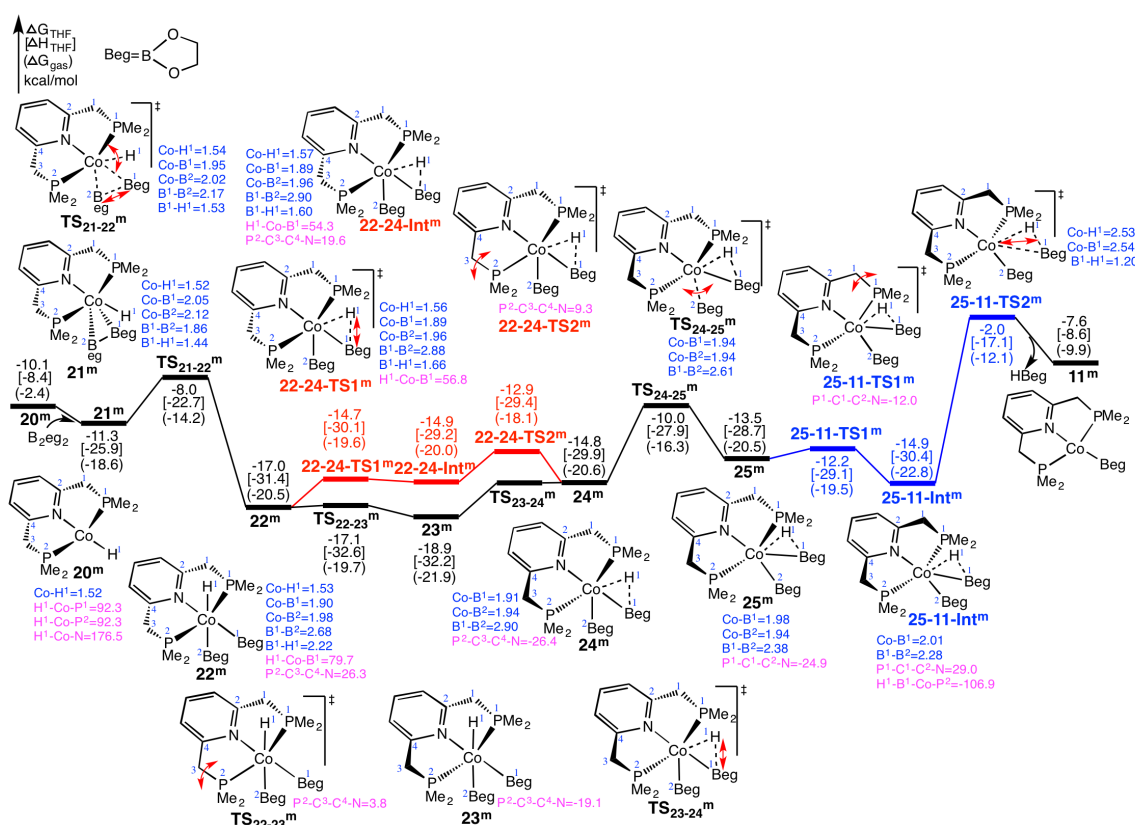


Figure S24: Calculated energy profiles for the regeneration of (<sup>Me</sup>PNP)CoBeg (**11<sup>m</sup>**) from (<sup>Me</sup>PNP)CoH (**20<sup>m</sup>**) and B<sub>2</sub>eg<sub>2</sub>.

Another alternative pathway with one phosphine ligand dissociated was considered here. Optimizations of the structures generated from the geometries of **21<sup>m</sup>** and **22<sup>m</sup>** by dissociating one phosphine ligand converged to **21<sub>openP<sup>m</sup></sub>** and **22<sub>openP<sup>m</sup></sub>** shown in Figure S25. The B-B bond is cleaved in **21<sub>openP<sup>m</sup></sub>**, as the

distance between two B atoms in **21<sub>openP<sup>m</sup></sub>** is longer than that in **21<sup>m</sup>**. Different from **22<sup>m</sup>**, the <sup>2</sup>PMe<sub>2</sub> ligand bends upside and the Beg groups are closer to the hydride in **22<sub>openP<sup>m</sup></sub>**. Relative to separated **20<sup>m</sup>** and B<sub>2</sub>eg<sub>2</sub>, the two complexes **21<sub>openP<sup>m</sup></sub>** and **22<sub>openP<sup>m</sup></sub>** (Figure S25) are calculated to be 6.4[-6.2](-1.8) and -0.7[-14.6](-8.1) kcal/mol, respectively, which are much higher than the stationary points involved in Figure S24. Thus, this possibility is unlikely.

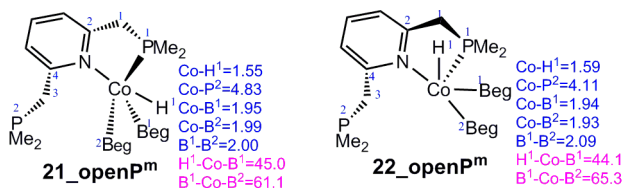


Figure S25: Structures for the complexes with one phosphine ligand dissociated that are related to complexes **21<sup>m</sup>** and **22<sup>m</sup>**.